

Confinement of surface patterning in azo-polymer thin films

Kevin G. Yager and Christopher J. Barrett

Department of Chemistry, McGill University, Montreal, Quebec H3A 2K6, Canada

(Received 30 November 2006; accepted 16 January 2007; published online 7 March 2007)

Azobenzene polymer thin films are known to spontaneously generate surface patterns in response to incident light gradients. This peculiar process is investigated in terms of the dynamics of the various azobenzene photomotions, which occur on different length scales. In particular, the formation and thermal erasure of surface relief gratings are measured as a function of film thickness and by using combinatorial samples with thickness gradients. The thermal erasure of gratings in this system provides a direct measure of the glass-transition temperature, which is found to deviate substantially from the bulk value. Thin azo films exhibit a glass transition up to 50 K higher than the bulk. These dynamical measurements allow the authors to probe the length scale of mass transport, which is found to be ~ 150 nm. Furthermore, surface mass transport is completely arrested in thin films < 40 nm. According to these results, mass transport involves the coordinated motion of many polymer chains in the depth of the sample, rather than surface diffusion of individual chains.

© 2007 American Institute of Physics. [DOI: 10.1063/1.2538787]

INTRODUCTION

Azobenzene polymers (hereafter “azo”) are unique materials that exhibit remarkable photophysical and photomechanical properties.^{1,2} Fundamentally, the azo chromophore undergoes a clean and efficient photoisomerization when irradiated with light anywhere within its broad absorption spectrum (see Fig. 1). This isomerization converts the stable *E* (*trans*) azo into a metastable *Z* (*cis*) azo state. The *cis* isomer will revert thermally back to the *trans* form, or this back isomerization can be photoinitiated. For the azo materials studied here (so-called pseudostilbenes), the thermal back relaxation has a time scale on the order of seconds, and since the *trans* and *cis* absorption spectra overlap, a single wavelength of light (in the region of 450–490 nm) can be used to induce both the forward and the reverse photoisomerization simultaneously. This molecular-scale photomotion leads to a host of larger-scale material motion effects. For instance, the azo chromophore can be photoaligned with polarized light due to a statistical absorption and reorientation phenomenon, where chromophores accumulate perpendicular to the incident polarization. This fully reversible chromophore alignment leads to strong dichroism and birefringence in the azo materials due to the azo’s anisotropic structure. The azo photomotion has been investigated as a photoswitch,³ to align liquid-crystalline systems,⁴ to bend freestanding thin films,⁵ and in many other photodynamic systems.²

In 1995, a further photomotion was discovered in the azo system.⁶ It was found that irradiation with a light intensity and/or polarization *gradient* would lead to spontaneous large-scale motion of polymer material in the thin film, resulting in surface topographical patterning. In the simplest experiment (see Fig. 2), the sample is exposed to a sinusoidal variation in light intensity, originating from the interference of two coherent laser beams. The end result is that the azo material generates a surface relief grating (SRG), as shown

in Fig. 2. Any incident light field can be used, with the azo material’s surface deforming to reproduce the light pattern. The process is strongly polarization dependent⁷ and occurs even at remarkably low laser power ($1\text{--}100$ mW/cm²). This topographical hologram is stable indefinitely at room temperature, but can be erased by heating the film past its glass-to-rubber transition temperature (T_g), in which case the original film thickness is recovered. This demonstrates that the process in question is a material motion, and not a photoablation phenomenon where material is lost, as would be the case for most materials irradiated at extremely high power. The periodicity of the grating is diffraction limited, being determined by the wavelength of light and the inscription geometry. For typical inscription conditions, a peak-to-peak spacing of 700 nm is obtained. Despite active investigation, the mechanism of this photopatterning phenomenon has not

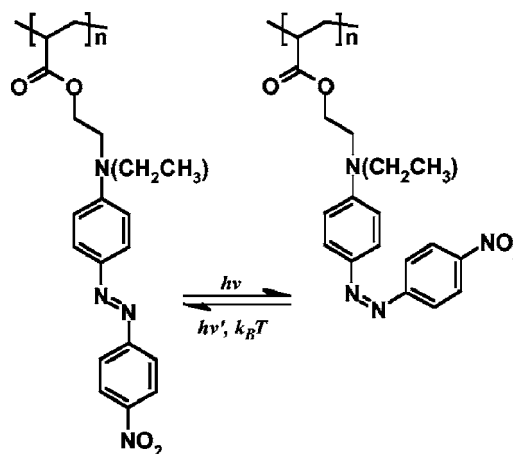


FIG. 1. Molecular structure of the azobenzene-containing polymer poly(disperse red 1 acrylate) (pdr1a). The azo chromophore isomerizes from the *trans* to the *cis* state when irradiated at an absorbing wavelength. The molecule relaxes thermally back to the stable *trans* state, or can be reconverted photochemically.

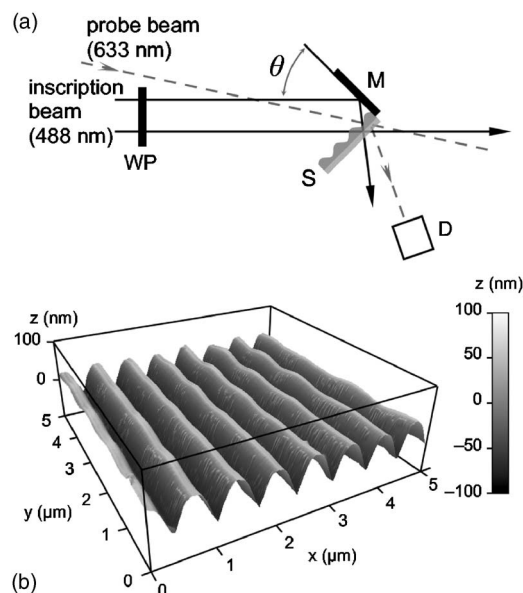


FIG. 2. (a) Experimental setup for inscription of surface relief gratings in azo thin films. The azo sample (S), cast on a glass slide is placed in proximity to a mirror (M). An inscription laser beam (Ar^+ 488 nm) is circularly polarized using a quarter-wave plate (WP). The laser beam reflects off of the mirror and interferes with itself at an angle θ . The grating formation can be measured in real time using a probe laser beam (HeNe 633 nm) that is diffracted into a detector (D). (b) The resulting sinusoidal surface relief grating, inscribed into the azo-polymer surface, as measured using atomic force microscopy.

been fully resolved.⁸ Suggested mechanisms include photopressure,⁹ asymmetric diffusion,¹⁰ mean-field forces,¹¹ and optical gradient forces.^{7,12} Not only is the fundamental origin of the driving force not elucidated but there are still unknowns related to the size-scale and dynamics of the mass transport phenomenon. The present paper attempts to probe these questions using dynamics measurements in films of varying thicknesses. In particular, we probe the efficiency SRG formation as a function of film thickness and measure the SRG erasure temperature in this thickness series.

Gratings in thin films can easily be quantified using the intensity of a diffracted probe laser beam. An azo material irradiated with a light interference pattern will have a number of superimposed gratings inscribed into it. During laser irradiation, the illuminated areas will have a higher *cis* fraction than the dark regions of the pattern. The *cis* and *trans* isomers have different refractive indices, and this spatially periodic refractive index produces a phase grating. This chemical grating is transient since it will decay after irradiation ceases (since the *cis* isomers will thermally revert to the *trans* form). In addition, the polarization-dependant orientation of azo chromophores will lead to a birefringence grating, since the birefringence (hence refractive index measured by the probe laser) is spatially varying. This grating is stable at room temperature, although it experiences a measurable decay after irradiation ceases due to orientational relaxation.¹³ The surface relief grating (topographical grating) is stable at room temperature. The diffraction efficiency of the SRG is very high, owing to the large-amplitude surface modification (up to hundreds of nanometers), and typically the measured diffraction efficiency is dominated by the

topographical grating component. More recently, evidence for a density grating inscribed beneath the surface of a SRG has been found.¹⁴ This grating was found to form during SRG inscription, but was only measurable after a subsequent thermal treatment step. Apparently the inscription process gives rise to seeding crystallites that grow with thermal treatment, leading to a spatially varying density in the material. This density grating in principle leads to spatial variation of refractive index. In practice, however, it makes only a small contribution to the visible-light diffraction efficiency (although it is readily measured using x-ray diffraction). Thus the visible-light diffraction efficiency is largely a probe of the surface relief, and the x-ray diffraction a measure of the density grating. The simultaneous existence of these coincident gratings (chemical, birefringence, topographical, and density) necessarily complicates the analysis of the diffraction efficiency. However it also provides for independent measures of material dynamics at different size scales. For instance, the chemical and birefringence gratings are related to molecular-scale motion (azo chromophore isomerization and orientation) whereas the topographical grating involves lateral length scales on the order of hundreds of nanometers.

Previous investigations have measured the temperature at which photoinduced orientation (i.e., birefringence) is erased.¹⁵ In these liquid-crystalline systems, the birefringence is stable above the glass-transition temperature, owing to the order of the liquid crystalline phase, but is erased at the melting temperature for the mesophase. In amorphous systems,¹⁶ it is not possible to maintain photo-orientation above T_g . Thermal erasure of azo-polymer surface relief gratings has recently been probed by simultaneous visible-light diffraction and x-ray diffraction.^{17,18} Erasure of the SRG was observed to coincide with the bulk glass-transition temperature in the thin films studied. Evidence was also found for the formation of a buried density grating during SRG formation, which becomes enhanced during the thermal treatment. To further this analysis, we now consider the erasure of surface relief gratings in thin films of varying thicknesses. The thickness dependence of the grating erasure provides information about the dynamics of the mass transport phenomenon and allows us to measure the length scale associated with the phenomenon.

EXPERIMENT

Sample preparation

The polymer material, poly[4'-[[2-(acryloyloxy)ethyl]ethylamino]-4-nitroazobenzene], usually referred to as poly-(disperse red 1 acrylate) (hereafter pdr1a) was synthesized as previously reported.¹⁹ This is a "push-pull" type of azomolecule, where the 4-position and 4'-position electron-donating and electron-withdrawing groups lead to high-efficiency photophysical effects. The azo-polymer pdr1a was selected due to its high efficiency in mass transport experiments, enabling sensitive measurement of transport efficiency. The present samples were prepared with a molecular weight of 3700 g/mol and were measured to have a glass-transition temperature (T_g) of 95–97 °C. Thin-film samples were prepared by spin coating azo-

polymer solutions (pdr1a in tetrahydrofuran, THF, solvent) onto cleaned glass microscope slides. The solution was placed on the substrate, and subsequently ramped (acceleration 1260 rpm/s) to 1300 rpm, and maintained for 35 s. The film thickness was varied by adjusting the concentration of the solution (in the range of 10^{-1} to 10^{-3} mol/l, based on repeat unit molecular mass). Thin films were annealed in a vacuum oven at 110 °C for 8 h to remove any residual solvent or flow-induced orientation. The film thickness was measured by imaging a scratch in the thin film by atomic force microscopy (AFM) (Digital Instruments Nanoprobe IIIa in contact mode and Asylum MFP-3D in tapping mode). Thickness measurements were corroborated by UV-vis spectroscopy and knowledge of the material extinction coefficient. Samples prepared with a thickness gradient were obtained using literature methods.²⁰ Briefly, a droplet of polymer solution is placed on a substrate, and a knife edge held above the surface is used to drag the solution across the substrate. Since the final film thickness depends on the drag velocity (as well as solution concentration), an acceleration ramp will generate a thin film with a thickness gradient. In this work, a 50 μ l drop of polymer solution (5×10^{-2} mol/l, based on repeat unit, pdr1a in THF) was coated onto cleaned glass microscope slides. The gap between the substrate and the blade was maintained at ~ 100 μ m, with a blade angle of 5°. The substrate was ramped from 1 to 5 mm/s at an acceleration of 0.56 mm/s².

SRG formation

SRGs were prepared by placing a thin film adjacent to a mirror, which reflected a coherent laser beam onto the surface (experimental setup shown in Fig. 2). Inscription was performed at room temperature (25 °C), and from previous work it is known that the low laser power used does not lead to appreciable sample heating.²¹ Laser inscription was performed using the 488 nm line of an argon-ion laser (Coherent Innova 308). Unless otherwise specified, the irradiation intensity was 37 mW/cm², the inscription angle was $\theta = 20^\circ$, and the irradiation time was 420 s. The incident laser beam was circularly polarized using a quarter-wave plate. Interference of right- and left-handed circularly polarized laser beams is known to give rise to high-efficiency surface relief formation. Grating amplitude during formation was quantified using the diffraction of a probe laser beam (20 mW HeNe 633 nm laser attenuated by a neutral density filter, absorbance 2.0). The height of the final inscribed surface relief grating was measured by AFM.

SRG erasure

Grating erasure experiments involved measuring the decay of the diffraction of a probe laser beam (10 mW HeNe 633 nm laser attenuated by an ND 2.0 filter) during thermal ramping. The probe beam was attenuated to minimize any possible photoisomerization or photo-orientation (absorption at 633 nm is small, yet can nevertheless lead to measurable photophysical effects²²). Furthermore, a computer-controlled shutter was synchronized with data acquisition, so that the probe beam illuminated the sample only when required. This

further minimized sample exposure to the probe beam during the long experiment duration (~ 24 h). The sample was fixed inside a heating stage with optical windows on the front and back (INSTEC HCS302), driven by a temperature controller (INSTEC STC200). Good thermal exchange between the sample and the heating block was ensured using metal contact spacers. The thin film was ramped from 25 to 140 °C (or 160 °C, as required) at a rate of 0.08 °C/min. This ramp rate was selected based on initial exploratory experiments, where it was determined that the erasure temperature depended on ramp rate if the rate was too high. For the slow ramp rate chosen, there is no longer any appreciable dependence on the rate.

Diffraction efficiency

The diffraction efficiency can be quantitatively related to the height of the induced surface relief grating and the intensity of the inscribed birefringence and density grating (which both give rise to a spatial variation of refractive index). Specifically, the intensity of the diffracted visible light, for the m th order diffraction, scales as²³

$$I \approx |J_m(q_z h) - e^{iq_z d} J_m(q_z \Delta n_m d)|^2, \quad (1)$$

where the J_m refer to the Bessel functions, h is the grating height (defined as the vertical distance between the peaks and valleys of the surface sinusoidal modulation), d is the film thickness, and Δn_m is the m th Fourier component of the refractive index grating. The scattering angles are contained in the momentum transfer,

$$q_z = n \frac{2\pi}{\lambda} (\cos \theta_i + \cos \theta_f), \quad (2)$$

where n is the refractive index, λ is the wavelength of the probe beam, and θ_i and θ_f refer to the incident and diffracted angles, respectively (as measured from the surface normal). These equations can be used to describe both the formation and erasure of a surface relief grating. The Bessel functions can give rise to oscillations in the diffracted signal. The grating heights employed in the present work, however, were kept beneath the first oscillation in the function, which simplifies data fitting.

During grating erasure, the diffraction efficiency is eliminated at a characteristic temperature. Thus the height of the SRG can be assumed to follow an equation of the form^{18,23}

$$h = h_{\max} \frac{1}{1 + \exp((T - T_{g,a})/E_a)}, \quad (3)$$

where $T_{g,a}$ is the apparent glass-transition temperature (erasure temperature), h_{\max} is the initial grating height (which can be determined from AFM), and E_a is an activation energy, which describes the breadth of the transition. A similar equation exists for the erasure of the Δn grating. However, the previous work on fitting grating erasure data has shown that the birefringence component is much smaller than the surface relief component, at least prior to a first melting sequence. It was confirmed here that the results are not appreciably affected if the refractive index grating (Δn term) is

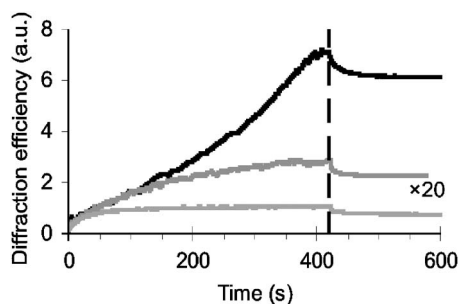


FIG. 3. Diffraction efficiency (arbitrary units) measured during grating inscription. The irradiation laser was turned on at 0 s and was turned off at the moment indicated by the dashed line (420 s). The upper curve is for a 427 nm film, the middle curve for a 114 nm film, and the lower curve for a ~ 20 nm film (these data have been scaled 20-fold for clarity).

ignored for the fits to the erasure data. Using the above equations, we were able to obtain high-quality fits to the thermal grating erasure data.

RESULTS AND DISCUSSION

Grating formation

The diffraction intensity of a probe laser beam (HeNe 633 nm) was measured during the inscription of surface relief gratings. Representative results can be seen in Fig. 3. As film thickness is decreased, the diffraction efficiency decreases considerably. Moreover, there is clear evidence that grating formation saturates more quickly in thinner films than it does in thicker films, indicating that material motion is being arrested in thinner films. The decay of the signal seen immediately after the laser is turned off is due to *cis* to *trans* back relaxation (i.e., elimination of the chemical grating) and some amount of orientational diffusion (i.e., relaxation of the birefringence grating).¹³ Both of these processes are molecular in origin. In particular, the decay portion of the data is well described by a biexponential function

$$\text{signal} = ae^{-k_{ct}t} + be^{-k_{or}t}, \quad (4)$$

where t is time after the inscription laser is turned off, $a = 0.22$ is the relative contribution from the chemical grating, and $b = 0.78$ is the relative contribution of the orientational grating. The value for the *cis* to *trans* relaxation is $k_{ct} = 0.24 \text{ s}^{-1}$, as reported previously in the literature.²⁴ The value for the orientational relaxation was fit to be $k_{or} = 0.063 \text{ s}^{-1}$. These same values can be used to fit the decay for films of all thickness values, indicating that these relaxation processes are not appreciably affected by thin-film confinement in the range of 20–430 nm. It is worth noting that a previous investigation²⁵ used the azobenzene *cis* to *trans* relaxation as a probe of mobility in thin polystyrene films. In that work, evidence for enhanced mobility of the isomerization (hence of the polymer network) was detected for thin films < 100 nm. This effect was not detected in the present study, although the postinscription relaxation has a substantial orientational component, which may be unaffected by film thickness in the range probed. In any case, it is evident that the molecular-scale processes are much less sensitive to the film thickness than the larger-scale mass transport phenomenon, as will be shown below.

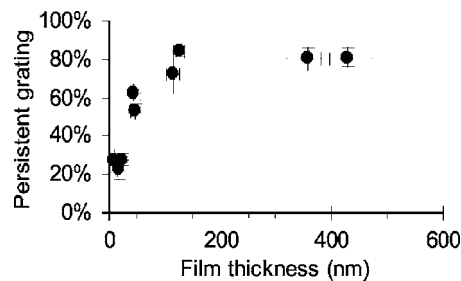


FIG. 4. Variation of the composition of the measured diffraction signal as a function of film thickness. The extent of the persistent grating (primarily surface relief) relative to the transient grating (primarily chemical) can be quantified using the diffraction efficiency data (see Fig. 3). In thick films, the diffraction is primarily due to the large-scale SRG, whereas in thin films the molecular-scale chemical grating dominates.

As discussed in the Introduction, laser irradiation generates several kinds of gratings simultaneously. Both a persistent grating and a transient grating are inscribed. The latter gives rise to the decrease in signal observed after irradiation ceases. The persistent grating results from topographical patterning (SRG) and the birefringence grating. Except in extremely thin samples, the topographical grating is the dominant contributor to the measured persistent diffraction. The transient grating, on the other hand, is due to the *cis/trans* chemical grating, with some contribution from the birefringence grating, which relaxes due to orientational diffusion after the laser is turned off. The SRG by contrast remains fixed after the laser is turned off and is not part of the observed transient signal. Thus the transient grating is a probe of molecular-scale motion (azo isomerization and azo dipole motion) whereas the persistent grating is a probe of larger-scale motion (involving mass transport of polymer chains). The relative contribution of the persistent and transient gratings can be seen in Fig. 4. These data provide a measure of the extent to which the various processes (molecular and larger-scale polymer motion) are affected as film thickness decreases. For thick films, the persistent grating (the SRG) accounts for the majority of the observed diffraction, whereas in thin samples it becomes the minor contribution. This indicates that as we scale to thinner samples, the formation of surface relief is being arrested more significantly than the molecular motions of *cis/trans* isomerization and orientational motion of azo dipoles. In other words, the larger-scale photomotions of the azo chromophore are being hindered, whereas molecular-scale photomotions are not. In fact, the absolute intensity of the transient grating decreases nearly linearly with decreasing film thickness, suggesting that it is not affected by confinement.

SRG height

In order to ascertain the scaling of SRG formation with film thickness, an azo thin film with a macroscopic gradient in thickness across its surface was exposed to interfering laser light (Fig. 5). This combinatorial experiment allows a range of thickness values to be probed simultaneously. The sample was illuminated with a gradient in light intensity, thereby creating a two-dimensional combinatorial sample that simultaneously probes film thickness and irradiation in-

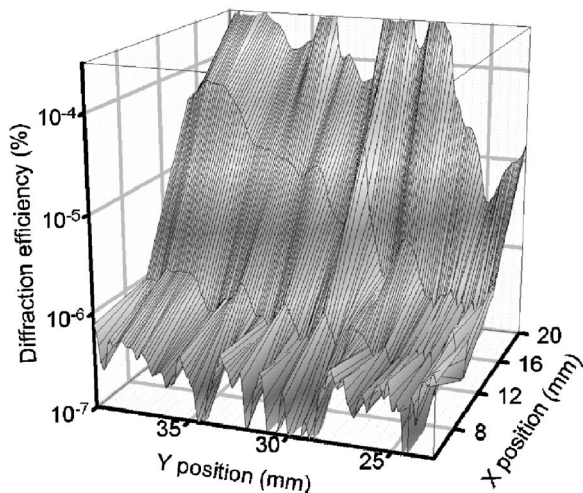


FIG. 5. Diffraction efficiency (logarithmic scale) for a combinatorial thin film of azo polymer. The sample thickness increases in the +Y direction. The sample was irradiated with a light interference pattern whose intensity increases in the +X direction.

tensity (and the interplay between these two parameters). As expected, the diffraction efficiency increases with increasing irradiation intensity (the intensity is 2.8 mW/cm^2 near $X=0 \text{ mm}$ and increases to 33.7 mW/cm^2 at $X=20 \text{ mm}$). It can also be seen that diffraction efficiency is larger in thicker films (film thickness varies from 30 nm near $Y=25 \text{ mm}$ to 60 nm near $Y=40 \text{ mm}$). Direct measurements of surface relief grating height were also conducted using AFM on a series of samples with different thickness values. The data, shown in Fig. 6, again demonstrate that grating inscription becomes hindered in extremely thin films, regardless of the laser intensity used. In extremely thin films ($<40 \text{ nm}$), the SRG height becomes smaller than the film roughness and is not detectable by AFM. This inability to form surface relief structures in ultrathin films suggests that a certain size scale of material motion is required for efficient mass transport. It should be emphasized that the reduction in grating thickness in thinner films is not merely a linear decrease. Specifically, the relative grating height (ratio of grating height to film thickness) increases as film thickness is decreased, until $\sim 130 \text{ nm}$, below which the relative grating height drops quickly towards zero. This trend suggests that grating formation is inhibited due to a critical size scale on the order of $40\text{--}150 \text{ nm}$.

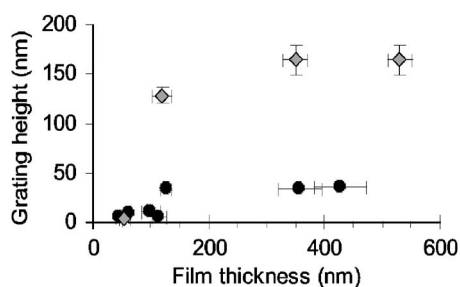


FIG. 6. Inscribed grating height (SRG amplitude) as a function of film thickness, as measured by AFM. The gray diamonds correspond to a laser irradiation intensity of 120 mW/cm^2 , whereas the black circles correspond to 37 mW/cm^2 . In both cases a decrease in grating height is seen in thinner samples.

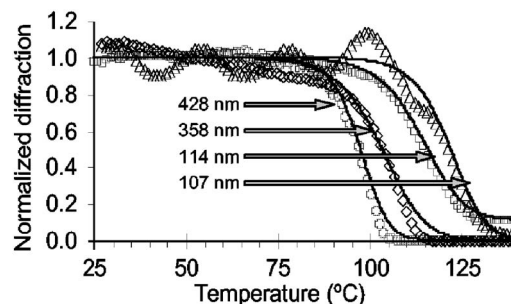


FIG. 7. Typical grating erasure curves for films of different thicknesses. The symbols are the experimental data and the solid lines are the fits. As the film thickness is decreased, the curve is shifted to higher temperatures, corresponding to a higher grating erasure temperature.

Grating erasure

To further probe the size-scale dependence of mass transport dynamics in the azo-polymer system, surface relief gratings were thermally erased. Typical grating erasure curves are shown in Fig. 7. As the thin film is heated, the diffraction efficiency eventually begins to drop due to material flow that serves to erase the grating. The oscillations observed in the signal can be attributed to thermal expansion of the film, sample substrate, and the optical windows in the sample enclosure. This explanation was confirmed in a control experiment where a thin film with a SRG was maintained at various temperatures. During temperature ramping, oscillations in the signal occur, whereas when the sample is held at a particular temperature the signal decreases slowly and without any oscillations. The oscillations are more pronounced in thinner films, since the absolute diffraction efficiency in these cases is smaller. The observed elimination of surface relief is undoubtedly a surface-tension driven process. At room temperature the material is an amorphous glass and material motion is impossible. As the glass-transition temperature is approached, coordinated polymer motions become activated and the thin film flattens out any surface patterns. The grating erasure data can be fit using Eqs. (1)–(3). The end result of such a fit is the determination of an erasure temperature ($T_{g,a}$) and an activation energy for the process (E_a). For thick films ($>350 \text{ nm}$), the erasure temperature corresponds well to the bulk glass-transition temperature (T_g). Specifically, the grating erasure occurs at $102 \text{ }^\circ\text{C}$, slightly higher than the bulk T_g of $95\text{--}97 \text{ }^\circ\text{C}$. It is worth noting that a decrease in diffraction is observed $\sim 15 \text{ }^\circ\text{C}$ before the $T_{g,a}$ is reached, which is $\sim 10 \text{ }^\circ\text{C}$ below the bulk T_g value.

Figure 7 shows a sample of grating erasure curves for films of different thicknesses. In all cases surface relief gratings were inscribed with identical optical irradiation parameters. As film thickness is decreased, the erasure temperature exhibits a remarkable shift towards higher temperatures. The fit parameters are shown in Fig. 8. The deviation from bulk T_g becomes very large in the thinnest films, with no indication of grating erasure even after passing through the bulk T_g value. For thin films of 46 nm , the measured $T_{g,a}$ is $\sim 50 \text{ }^\circ\text{C}$ higher than the bulk glass transition. This represents a substantial shift of the film dynamics compared to bulk samples, evidently related to thin-film confinement. The breadth of the

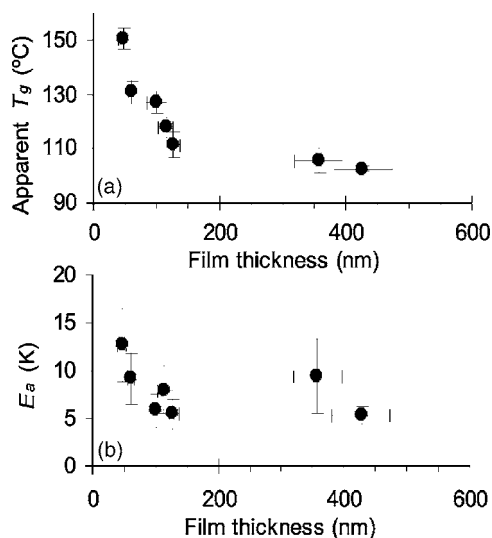


FIG. 8. Fit parameters for grating erasure data for various film thickness values. (a) The apparent T_g (grating erasure temperature) increases dramatically in thin films <150 nm. (b) The breadth of the erasure (described by E_a) is a comparatively insensitive parameter and does not vary considerably as a function of film thickness.

transition (described by E_a) is a comparatively insensitive fit parameter. It does not appear to follow any trend with film thickness, with a value of ~ 8 K reasonably describing all the data.

It is important to emphasize that the change in apparent T_g with film thickness cannot be explained by SRG height alone. For example, in the thinnest films the inscribed gratings are of nearly equal height, yet the apparent T_g is nevertheless strongly sensitive to film thickness in this regime. As a further check, SRGs of various heights were inscribed in films, using different irradiation times. The grating erasure temperature was found to depend on the film thickness, and not the height of the SRG being erased.

Ultrathin films

In extremely thin films (<40 nm), any inscribed surface relief grating is essentially nonexistent, as measured by AFM, being smaller than the roughness of the sample surface. In these ultrathin films, one can nevertheless measure a small rise in diffraction efficiency during laser inscription and an erasure of this diffraction during the temperature ramping step. In this case, the observed grating is likely entirely due to the inscribed birefringence grating. In extremely thin films (<40 nm), the birefringence grating is erased at ~ 110 °C, which corresponds to the sample's bulk glass-transition temperature. We can again conclude that the molecular-scale motion of azo orientation is not affected by thin-film confinement effects, in marked contrast to the large-scale surface mass transport. Undoubtedly the erasure of the birefringence grating is occurring in samples >40 nm as well, but this erasure appears to be small in size compared to the erasure of the SRG, whose diffraction efficiency is much larger. In fact the gradual decrease in diffraction efficiency as T_g is approached in thicker samples can be attributed to erasure of the weak birefringence grating. Thus for thicker samples (>40 nm) the erasure is dominated by the topo-

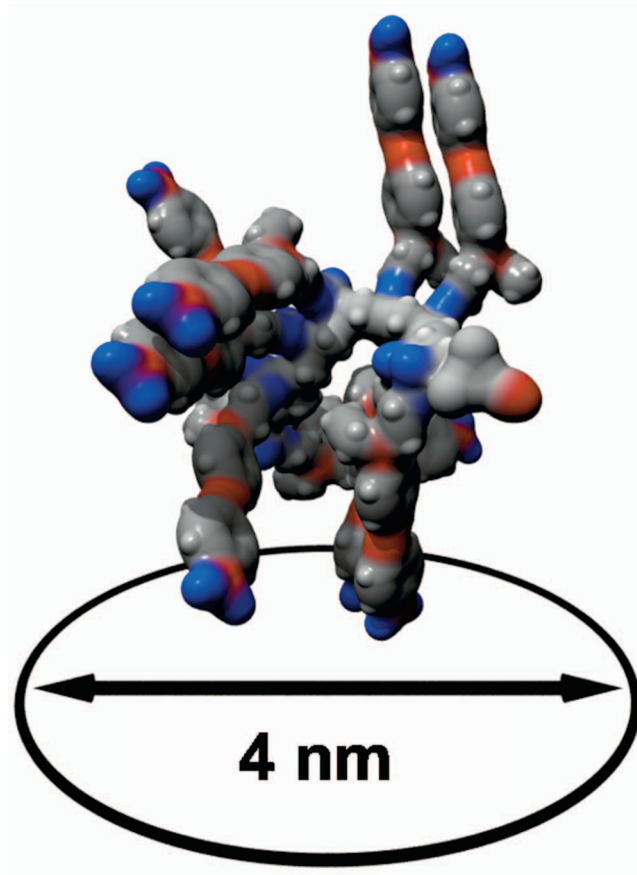


FIG. 9. (Color) Molecular model of a typical pdr1a azo-polymer chain (10 repeat units). The size of a polymer chain is quite small: on the order of 3–4 nm.

graphical grating (with a small contribution from a birefringence grating), whereas in thinner samples (<40 nm) the topographical grating cannot be written and the observed diffraction is entirely due to the birefringence grating.

The inability to form gratings in ultrathin samples is not merely a limitation of irradiation power or time. From Fig. 6 we can see that even with greater irradiation power, the SRG height decreases to zero near ~ 40 nm. Furthermore, the grating inscription curves (Fig. 3) show faster saturation for the thinner samples, with no further rise in the signal, indicating that even with further irradiation, no SRG would be produced. This was confirmed with extremely long irradiation times (several hours), where no grating could be generated in ultrathin films. The inability to form gratings in ultrathin samples is an indication of the size scale of material motion required to generate an SRG.

Mass transport sizescale

The data clearly indicate that the SRG formation and erasure involve motion over a length scale on the order of 150 nm. This size scale is much larger than the azo molecule. The azo polymers used for surface patterning are typically low molecular weight chains. In the present study, the polymer molecular weight was approximately 3700 g/mol, corresponding to chains that are 8–12 repeat units long. A minimized molecular model of a 10-mer is shown in Fig. 9

(generated using the Amber Force Field method from the HYPERCHEM 6.0, Hypercube Inc. software). The size of a typical polymer chain in this system is on the order of 3 nm, considerably smaller than the 150 nm length scale involved in mass transport. Thus the inhibition of dynamics seen in thin films is not a polymer-chain confinement effect. Instead, the material transport appears to involve the coordinated motion of many polymer chains. Such an effect is more naturally described in a hydrodynamic framework. The polymer-substrate interface acts as a pinning surface, preventing material motion at that point. This frictional force prevents material motion well into the material. This effect is in some ways similar to a fluid boundary layer (although by any conventional calculation, the size of the boundary layer in this case is orders of magnitude larger than the film thickness).

Surface chemistry

If the increase in erasure temperature is due to interaction with the substrate, it is natural to ask whether altering the surface chemistry will affect the observed trends. Glass slides treated with dimethyldichlorosilane present a highly hydrophobic CH_3 terminate surface. In this case the affinity of the polymer for the surface is decreased, and as a result the thin film was found to undergo significant dewetting. Conversely, a glass slide treated with piranha cleaning solution (boiling 3:1 mixture of H_2SO_4 and H_2O_2) presents an oxidized, OH rich, and thus hydrophilic, surface. In this case the polymer does not dewet, but surface affinity is again decreased. As with the untreated glass surfaces, no grating inscription in thin films <40 nm was observed on the highly hydrophilic glass substrates. Whether or not the scaling of the apparent T_g is modified by different surface chemistries (or indeed in freestanding thin films) is an open question that bears further study.

Glass-transition temperature

It is now well established that thin freestanding polymer films exhibit depressed T_g relative to the bulk value.²⁶ This effect has been mapped through the thickness of thin polymer films,²⁷ where it was determined that the free surface of a polymer film exhibits enhanced dynamics relative to the bulk. This effect was found to penetrate ~ 20 nm into polystyrene thin films. The existence of this mobile surface layer, combined with the present data, allows us to rigorously exclude a purely surface-layer mass transport phenomenon in azobenzene systems. If the material motion were occurring purely at the surface, the erasure of a SRG would be expected to occur at a $T_{g,a}$ considerably below the bulk value (i.e., it should occur at the T_g for the surface layer). Instead what is observed here is that even in the thickest films, the grating is erased near the bulk T_g value. This may be because the surface of these materials does not exhibit substantial deviations from bulk T_g (possibly due to the low molecular weight). However this may also be viewed as substantiation that the length scale for this material motion is much larger than this mobile surface layer.

The method presented in this paper for measuring dynamics, namely, to identify the erasure temperature for a sur-

face relief grating by measuring diffraction, could be applied to a wide variety of systems. In the case of azo polymers, the formation of a surface relief is especially straightforward due to the optical patterning process. However, in principle nearly any material could have a SRG inscribed onto it in some way, and the diffraction efficiency as a function of temperature could be used to measure the film dynamics. Previous investigations have measured the decay of nanoscale roughness²⁸ or embossed surface patterns²⁹ by AFM. Such measurements are obviously laborious, whereas measurement of diffraction efficiency is facile and sensitive. The method of hot-embossing surface patterns into polymer films could be applied to a wide range of systems, allowing for a new and direct measurement of relaxation phenomena in thin films. Moreover, novel measurements could be performed. For instance, two-dimensional surface patterns could be imprinted into a film, and the diffraction of a probe beam in the two orthogonal directions could be used to probe anisotropic dynamical properties.

An interesting avenue for future investigation would be to analyze the effect of molecular weight on the observed deviations of $T_{g,a}$. The azo surface patterning motion is known to be arrested in extremely high molecular weight systems and to be inefficient in monomeric systems. Within the regime of observable surface patterning, one would expect increased molecular weight (and associated chain dimensions) to lead to further hindering of dynamics and perhaps more substantial deviations of $T_{g,a}$. It should be noted, however, that established glass-transition anomalies²⁶ in thin polystyrene films were largely insensitive to molecular weight (within experimental error) in the low-molecular-weight regime. At higher molecular weight, the size scale of the inferred dynamics were indeed measurably greater as molecular weight was increased.

In the azo-polymer system, we have used the erasure of an inscribed grating to probe deviations from bulk T_g in thin film. We have measured substantial deviations from the bulk glass-transition behavior in thin films <150 nm. For extremely thin films (<50 nm), it would appear that the effective T_g of the thin film is ~ 50 °C higher than the bulk value.

CONCLUSIONS

Based on the presented results, it is clear that the long-range (hundreds of nanometers) motion of polymer material in azo samples is hindered in thin films due to confinement and the pinning effect of the substrate interface. Furthermore, the photoinduced mass transport phenomenon seen in the azobenzene system is arrested in extremely thin films, showing that this process is a long-range effect. In addition to substantial material flow in the film plane directions, it is now clear that the azo photomotion absolutely requires coordinated motion of material in the film normal direction, over length scales of ~ 150 nm.

Previous reports in the literature have analyzed the dynamics of the surface mass transport phenomenon. In particular, an experiment was performed where a thin film of azo material was capped with a thin transparent polyelectrolyte layer.³⁰ This thin layer of material was found to notice-

ably hinder grating formation. Combined with the present results, we now have a more complete and consistent picture of the nature of the mass transport phenomenon. In both cases, the results indicate that pinning azo motion (whether at the free surface or at the substrate) inhibits grating formation. The present experiments additionally provide evidence that material motion over larger length scales (~ 150 nm) in the film normal direction is required to move material at the sample surface. Furthermore, the efficiency of this process is strongly sensitive to the amount of material beneath the free surface, and not merely the material in proximity to the surface. This demonstrates that the material motion is not localized to the interface, but involves forces and material flow originating at greater distances. This explanation is consistent with the previous study, since capping the free surface of the thin film would be expected to hinder SRG formation due to the higher energy requirement for increasing film surface area. Adding a capping layer to an azo thin film creates a pinning interface analogous to the substrate pinning observed in this study.

With regard to the mechanism of surface relief formation, the present results are most consistent with a hydrodynamic and photomechanical model, such as the photoinduced pressure mechanism. Diffusion models, on the other hand, would predict that the process would occur efficiently in a thin surface layer and would not require coordinated motion within the film bulk. Similarly, models proposing localized forces between azo molecules would not predict a strong thickness dependence to the phenomenon. Instead what is observed here is that a long-range stress buildup in the film is responsible for the observed mass transport. Grating inscription is a manifestly large-scale phenomenon, both in terms of lateral material flow and in the film normal direction, where cooperation of material over nanometer to micron length scales is required for efficient photoinduced surface patterning.

ACKNOWLEDGMENTS

The authors thank Faisal Aldaye for help with molecular modeling, Derek Gray and Emily Cranston for help with the AFM work, Nasir Ahmad for materials synthesis, and Shing Kwok for performing initial exploratory experiments. Research funds were provided by NSERC Canada and the Canadian Foundation for Innovation.

¹A. Natansohn and P. Rochon, Chem. Rev. (Washington, D.C.) **102**, 4139 (2002).

²K. G. Yager and C. J. Barrett, J. Photochem. Photobiol., A **182**, 250 (2006).

- ³R. H. El Halabieh, O. Mermut, and C. J. Barrett, Pure Appl. Chem. **76**, 1445 (2004).
- ⁴K. Ichimura, Chem. Rev. (Washington, D.C.) **100**, 1847 (2000); Y. L. Yu and T. Ikeda, J. Photochem. Photobiol. C **5**, 247 (2004).
- ⁵T. Ikeda, M. Nakano, Y. Yu, O. Tsutsumi, and A. Kanazawa, Adv. Mater. (Weinheim, Ger.) **15**, 201 (2003); Y. Yu, M. Nakano, and T. Ikeda, Nature (London) **425**, 145 (2003).
- ⁶P. Rochon, E. Batalla, and A. Natansohn, Appl. Phys. Lett. **66**, 136 (1995); D. Y. Kim, S. K. Tripathy, L. Li, and J. Kumar, *ibid.* **66**, 1166 (1995).
- ⁷N. K. Viswanathan, S. Balasubramanian, L. Li, S. K. Tripathy, and J. Kumar, Jpn. J. Appl. Phys., Part 1 **38**, 5928 (1999).
- ⁸K. G. Yager and C. J. Barrett, Curr. Opin. Solid State Mater. Sci. **5**, 487 (2001).
- ⁹C. J. Barrett, A. L. Natansohn, and P. L. Rochon, J. Phys. Chem. **100**, 8836 (1996); C. J. Barrett, P. L. Rochon, and A. L. Natansohn, J. Chem. Phys. **109**, 1505 (1998).
- ¹⁰P. Lefin, C. Fiorini, and J. M. Nunzi, Opt. Mater. (Amsterdam, Neth.) **9**, 323 (1998); Pure Appl. Opt. **7**, 71 (1998).
- ¹¹T. G. Pedersen and P. M. Johansen, Phys. Rev. Lett. **79**, 2470 (1997); T. G. Pedersen, P. M. Johansen, N. C. R. Holme, P. S. Ramanujam, and S. Hvilsted, Phys. Rev. Lett. **80**, 89 (1998).
- ¹²J. Kumar, L. Li, X. L. Jiang, D. Y. Kim, T. S. Lee, and S. Tripathy, Appl. Phys. Lett. **72**, 2096 (1998); S. P. Bian, W. Liu, J. Williams, L. Samuelson, J. Kumar, and S. Tripathy, Chem. Mater. **12**, 1585 (2000); O. Baldus and S. J. Zilker, Appl. Phys. B: Lasers Opt. **72**, 425 (2001).
- ¹³T. Matsui, S. Yamamoto, M. Ozaki, K. Yoshino, and F. Kajzar, J. Appl. Phys. **92**, 6959 (2002).
- ¹⁴U. Pietsch, P. Rochon, and A. Natansohn, Adv. Mater. (Weinheim, Ger.) **12**, 1129 (2000); T. Geue, O. Henneberg, J. Grenzer, U. Pietsch, A. Natansohn, P. Rochon, and K. Finkelstein, Colloids Surf., A **198–200**, 31 (2002).
- ¹⁵P. S. Ramanujam, C. Holme, S. Hvilsted *et al.*, Polym. Adv. Technol. **7**, 768 (1996).
- ¹⁶O. K. Song, C. H. Wang, and M. A. Pauley, Macromolecules **30**, 6913 (1997).
- ¹⁷T. Geue, M. Schultz, J. Grenzer, U. Pietsch, A. Natansohn, and P. Rochon, J. Appl. Phys. **87**, 7712 (2000).
- ¹⁸T. M. Geue, M. G. Saphiannikova, O. Henneberg, U. Pietsch, P. L. Rochon, and A. L. Natansohn, J. Appl. Phys. **93**, 3161 (2003).
- ¹⁹A. Natansohn, P. Rochon, J. Gosselin, and S. Xie, Macromolecules **25**, 2268 (1992).
- ²⁰J. C. Meredith, A. P. Smith, A. Karim, and E. J. Amis, Macromolecules **33**, 9747 (2000); J. C. Meredith, A. Karim, and E. J. Amis, Macromolecules **33**, 5760 (2000); A. P. Smith, J. F. Douglas, J. C. Meredith, E. J. Amis, and A. Karim, J. Polym. Sci., Part B: Polym. Phys. **39**, 2141 (2001).
- ²¹K. G. Yager and C. J. Barrett, J. Chem. Phys. **120**, 1089 (2004).
- ²²C. Kempe, M. Rutloh, and J. Stumpe, J. Phys.: Condens. Matter **15**, S813 (2003).
- ²³U. Pietsch, Phys. Rev. B **66**, 155430 (2002).
- ²⁴C. Barrett, A. Natansohn, and P. Rochon, Chem. Mater. **7**, 899 (1995).
- ²⁵K. Tanaka, Y. Tateishi, and T. Nagamura, Macromolecules **37**, 8188 (2004).
- ²⁶J. A. Forrest and K. Dalnoki-Veress, Adv. Colloid Interface Sci. **94**, 167 (2001).
- ²⁷C. J. Ellison and J. M. Torkelson, Nat. Mater. **2**, 695 (2003).
- ²⁸T. Kerle, Z. Q. Lin, H. C. Kim, and T. P. Russell, Macromolecules **34**, 3484 (2001).
- ²⁹E. Buck, K. Petersen, M. Hund, G. Krausch, and D. Johannsmann, Macromolecules **37**, 8647 (2004).
- ³⁰N. K. Viswanathan, S. Balasubramanian, L. Li, J. Kumar, and S. K. Tripathy, J. Phys. Chem. B **102**, 6064 (1998).